In vivo optical resolution photoacoustic microscopy using glancing angle-deposited nanostructured Fabry–Perot etalons

Hajireza, Parsin; Sorge, Jason; Brett, Michael; Zemp, Roger

Publisher's version / Version de l'éditeur:
https://doi.org/10.1364/OL.40.001350
Optics Letters, 40, 7, pp. 1350-1353, 2015

In vivo optical resolution photoacoustic microscopy using glancing angle-deposited nanostructured Fabry–Perot etalons

Parsin Hajireza,[1] Jason Sorge,[1] Michael Brett,[1,2] and Roger Zemp[1,*]

[1]*Department of Electrical and Computer Engineering, University of Alberta, Edmonton, Alberta T6G 2V4, Canada*

[2]*National Institute for Nanotechnology, Edmonton, Alberta T6G 2M9, Canada*

**Corresponding author: rzemp@ualberta.ca*

Received November 26, 2014; revised January 29, 2015; accepted February 25, 2015;
posted February 25, 2015 (Doc. ID 228590); published March 23, 2015

In this Letter, reflection-mode optical resolution photoacoustic microscopy (OR-PAM) using glancing angle-deposited (GLAD) nanostructured Fabry–Perot interferometers (FPI) for *in vivo* applications is reported. GLAD is a single-step physical vapor deposition (PVD) technique used to fabricate porous nanostructured thin films. Using titanium dioxide, a transparent semiconductor with a high refractive index ($n = 2.4$), the GLAD technique can be employed to fabricate samples with tailored nano-porosity, refractive index periodicities, and high Q-factor reflectance spectra. The OR-PAM *in vivo* images of chorioallantoic membrane (CAM) of 5-day chicken embryo model are demonstrated. The phantom study shows lateral resolution and signal-to-noise ratio better than 7 μm and 35 dB, respectively. The sensitive GLAD FPI allows photoacoustic imaging down to a few-nJ pulse energy. To the best of our knowledge, this is the first time that a FPI-based reflection mode optical resolution photoacoustic imaging technique is demonstrated for *in vivo* applications.

OCIS codes: (180.0180) Microscopy; (180.5810) Scanning microscopy; (170.1065) Acousto-optics; (170.3880) Medical and biological imaging; (170.5120) Photoacoustic imaging.

http://dx.doi.org/10.1364/OL.40.001350

In photoacoustic imaging (PA) systems, absorbed optical energy is converted into acoustic signals by thermoelastic expansion and then received by ultrasound detectors to be processed into final images. PA imaging is capable of providing absorption contrast, enabling estimation of blood oxygen saturation, imaging of optical contrast agents, and imaging of gene expression, among other applications [1,2]. Most ultrasound and PA techniques employ piezoelectric receivers to detect the ultrasonic signals. However, all-optical ultrasound detection is desirable in applications such as intraoperative, laparoscopic, and endoscopic ultrasound image guidance systems. In these applications, electrical interconnects must be minimized, and integration of PA with existing optical methods will be facilitated. Recently, optical detectors have been under intense investigation for use in PA imaging [3–10]. Previous work on optical-based ultrasound detection includes Fabry–Perot interferometer (FPI), micro-ring resonators (MRRs), and other types of interferometric sensing. Adapting these methods for reflection-mode optical-resolution photoacoustic microscopy has been challenging. Most MRRs fabricated on silicon substrates are optically opaque [4], therefore, to image in reflection mode, the MRR and the optical scanning area need to be physically far from each other, or the resulting PAM system could be implemented in transmission configuration, which is not practical for imaging thick biological samples. Recently, a miniaturized, optically-transparent ultrasonic detector was developed [8]. However, only phantom imaging was demonstrated. Even with such a transparent substrate, the micro-ring resonator was in a different lateral location than the optical scanning. Other interferometric sensing approaches including Fabry–Perot-based methods have yet to achieve *in vivo* reflection-mode optical-resolution imaging. In our approach, the effective optical sensing area on the FPI is scanned with the excitation spot as close to the source as possible. This co-scanning of excitation and probe beams can be critical for high-signal-to-noise ratio *in vivo* imaging. Challenges of all-optical PA imaging with optical resolution include damage thresholds, co-alignment of excitation and interrogation beams, and ensuring adequate *in vivo* sensitivity for low pulse energies.

In this Letter, we demonstrate a FPI-based ultrasound detector fabricated using glancing angle deposited (GLAD) nanostructured thin films for *in vivo* optical resolution PA imaging. The nanostructured GLAD is a single-step physical vapor-deposition (PVD) technique used to fabricate nanostructured-thin films [11]. By employing substrate motion and obliquely incident vapor flux, characteristic porous arrays of columnar structures can be produced from a range of organic, semiconductor, and dielectric materials.

Using materials such as titania (TiO_2), a wide band gap and transparent semiconductor with a high refractive index ($n = 2.4$), the GLAD technique can be used to fabricate samples with tailored refractive index periodicities with a high level of control and hence provide high-Q-factor reflectance spectra. Other transparent materials such as silicon dioxide and magnesium fluoride could also be used, but FPIs fabricated with these materials would have a lower refractive index contrast due to lower bulk indexes than TiO_2. By periodically altering the deposition angle, and thus the local density and refractive index of deposited columns sublayers, GLAD photonic crystals (PCs) can be created with periodic wavelength-scale structure and resonant Bragg reflection [11].

We have previously showed the first GLAD FPI for ultrasound detection for phantom imaging in transmission mode [7]. The minimum detectable acoustic pressure of this glass-backing sensor was measured as 80 ± 20 Pa

and the –3 dB bandwidth was measured to be 18 MHz. GLAD films offer some practical and performance advantages over previous methods for ultrasound detection as it allows low acoustic-impedance FPI-device fabrication for highly sensitive ultrasound detection [7]. In this Letter, we report *in vivo* reflection-mode optical-resolution photoacoustic microscopy (OR-PAM) with FP etalons. Reflection-mode imaging presents new challenges because (1) excitation light is optically focused through the etalon, and high focal intensities can damage the etalon. (2) Ideally the excitation beam should be focused into the tissue, while the probe beam should be focused into the etalon, and this is not straightforward with a single objective lens for both beams. Our approach involves both optimization of the etalon and an optical design that permits scanning of both the excitation beam and interrogation beam together. This not only provides optimal sensitivity detection but also limits laser-dwell time on any one spot to prevent etalon damage.

Figure 1 systematically depicts the experimental setup of GLAD OR-PAM. This system consists of two main arms, receiver and excitation arms. Both beams are co-scanned and co-focused on the sample. In the receiver arm, a tunable continuous wavelength (CW) C-band laser (TLK-L1550R, Thorlabs Inc., New Jersey) was used in order to tune the interrogation laser wavelength to the point of maximum slope on the FPI peaks. The light at the laser aperture was coupled to a single-mode fiber and collimated. This collimated interrogation beam was passed through a polarized beam splitter (VBA05-1550, Thorlabs Inc., New Jersey) and $\lambda/4$ zero-order wave plate (Thorlabs Inc., New Jersey), onto the sample via a focusing objective lens, and back through the wave-plate creating 90° polarization, which then reflects at the polarizing beam-splitter in order to guide the maximum possible intensity of reflected light to a 150-MHz-bandwidth InGaAs photodiode (PDA10CF, Thorlabs Inc., New Jersey). An objective lens (518125, LEICA, Germany) was used in front of the photodiode in order to refocus all possible reflected interrogation light to the small photodiode element. The 30-mW interrogation beam was focused on the GLAD-FPI. The output of the photodiode was amplified (Olympus 5900PR) and digitized using a 4-channel PCI digitizer (Gage card) at a sampling rate of 200 MSamples/s.

In the excitation arm, the output of a 1-ns pulse width, ytterbium-doped fiber laser (IPG Photonics) with a pulse repetition rate (PRR) of 40 kHz was initially coupled into a 6-m PM-SMF to generate stimulated Raman scattering (SRS) peaks [12]. A band pass filter can be used in order to select the desired wavelength. The output of the PM-SMF was collimated using an adjustable collimator and combined by the receiver arm of the system. A 532-nm wavelength was selected for all the images shown in this manuscript. Unlike the previous design both beams are scanned across the samples using a 2D galvanometer scanning mirror system and focused tightly using an objective lens (Leitz Wetzlar 10X/0.25 160/- EF microscope objective, Germany). Also a band pass filter was used in front of the photodiode in order to reject the reflected 532-nm light.

Figure 2(a) shows the configuration of Fabry–Perot interferometers (FPI). The FPI was fabricated by growing multilayer optical filters using GLAD process. Figure 2(b) shows transmission spectrum of the GLAD FPI showing sharp resonant peaks near the C-band. Multilayer films were designed to have high transmittance at 532 nm and high reflectance at about 1550 nm. Figure 2(c) shows scanning electron microscope (SEM) image of the first GLAD layer. For this work, TiO_2 was

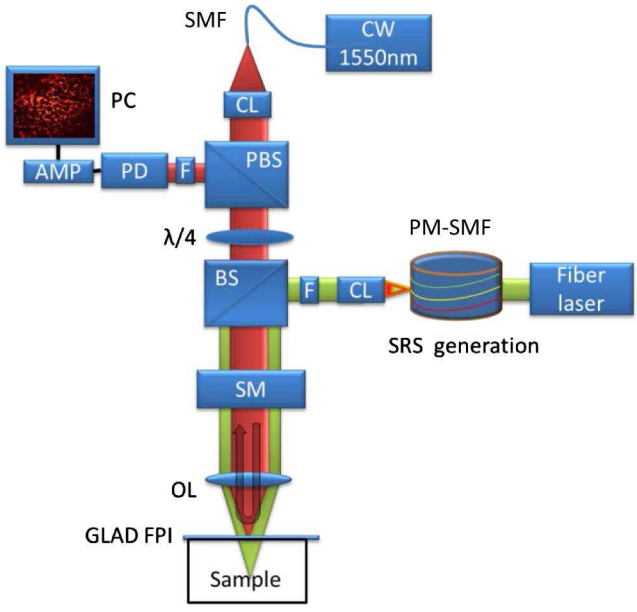

Fig. 1. Experimental setup of GLAD OR-PAM. F, filter; OL, objective lens; PMf-SMF, polarization-maintaining single-mode fiber; CL, collimator lens; PBS, polarized beam splitter; BS, beam splitter; SM, 2D scanning mirrors; PD, photodiode; AMP, amplifier.

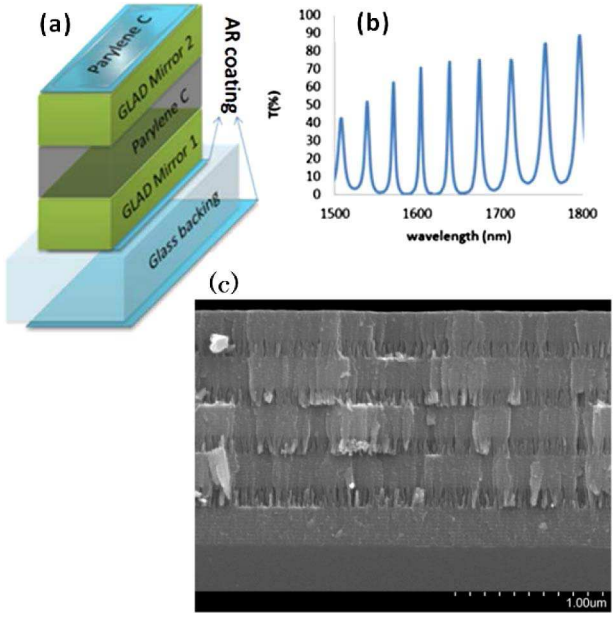

Fig. 2. (a) The configuration of FPI. AR (anti-reflection). (b) Transmission spectrum of the GLAD FPI showing sharp resonant peaks near the C-band. (c) SEM image of first GLAD layer. Dense layers were deposited at an angle of $\alpha = 60°$. Sparse, columnar layers were deposited at an angle of $\alpha = 80°$.

used as the deposition material, due to its high refractive index and transparency at the wavelengths of interest. High reflectance was achieved through the use of high/low-index stacks at deposition angles of $\alpha = 60°$ and $\alpha = 80°$, respectively.

At higher deposition angles, a more porous structure is grown, with a lower refractive index. When designing a reflecting medium at C-band consisting solely of quarter-wave layers, a higher order reflectance band was found to occur at 532 nm, which is undesirable. To correct this, the thicknesses of the high- and low-index layers were adjusted to shift the higher order reflectance band off of 532 nm, while keeping the initial reflectance band at 1550 nm intact. The effective indices of the high- and low-index layers were found to be $n_{60} = 1.93$ and $n_{80} = 1.42$, respectively. Half-wave plate antireflection coatings at 1550 nm were grown to increase the optical power coupled through the substrate and into the FPI.

The first step in the FPI fabrication process involved depositing a multilayer GLAD film to act as the first mirror. Electron beam evaporation (Axxis, Kurt J. Lesker Inc.) was used to deposit amorphous TiO_2 (Cerac Inc., rutile phase, 99.9% pure) onto microscope cover slips (Fisherbrand Microscope Cover Glass #1) with ~250 μm thickness. The substrates were adhered to a metal substrate holder that was connected to two rotation motors. The deposition angle was controlled by one motor, while the substrate rotation was controlled by a second motor. Each high refractive index layer consisted of 10 complete substrate rotations at a constant deposition angle of $\alpha = 60°$ over a 270-nm thickness. Low index layers consisted of 10 substrate rotations at a constant deposition angle of $\alpha = 80°$ over a 170-nm thickness. Each FPI mirror consisted of alternating four high- and low-index layers and ending with a dense layer. An extra dense layer was used to provide the best interfaces with the substrate and subsequent deposition layers. After the first multilayer film was fabricated, it was oxidized in an oven at 200°C for 24 h to achieve best transparency.

A 23-μm-thick Parylene-C layer was deposited by vapor deposition (PDS 2010, Lab Coater 2, University of Alberta Nanofabrication Facility) on top of the first multilayer GLAD film. Following the deposition of Parylene-C, a second multilayer GLAD film was deposited in the same manner as the first. Following this deposition, the samples were oxidized in an oven at 80°C for 120 h, to preserve the Parylene-C layer. Afterward, a 4-μm Parylene-C capping layer was used to encapsulate the entire sample to protect it from humidity and other environmental effects. Finally, unlike our previous approach, a half-wave layer antireflection coating consisting of a 315-nm-thick layer of SiO_2 (Materion, 99.99% pure) was deposited on the backside of the substrate to improve the optical coupling to the FPI. The optimized etalon exhibited FP peaks with optical Q-factors of 870, more than 40% higher than our previous work.

Figure 3 shows GLAD OR-PAM images of carbon fiber networks. Each individual carbon fiber has a diameter ~7 μm. The excitation pulse energy was set to 30 and 1 nJ on Figs. 3(a) and 3(b), respectively. The integration power on the FPI was measured ~10 mW. Detected signal levels displayed a linear relationship with pulse energy. The optical lateral resolution was estimated

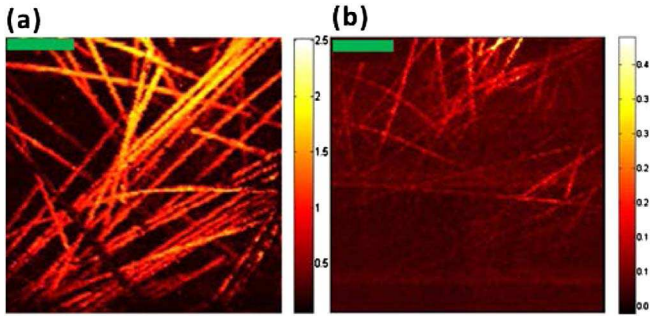

Fig. 3. GLAD OR-PAM images of carbon fiber network. Images are formed using a pulse energy of (a) 30 nJ, (b)1 nJ. (Scale bar: 100 μm.)

~7 μm [13]. Both images are formed using a 3 mm × 3 mm FPI. The small footprint and high sensitivity of the FPI makes this system a promising method for OR-PAM handheld and endoscopy applications [14,15].

Presently the FOV is limited to around 2 mm, where spherical aberrations of the objective lens degrade image quality far from the center axis. Also, etalon uniformity is problematic when scanning over larger areas and would require interrogation-beam wavelength tuning. Etalon uniformity has been problematic for other reported FPI sensors. As shown before in our work [7], the optimum interrogation wavelength (corresponded to the steepest slope on the reflectivity spectra) varies by only less than 1 nm over a 1 mm × 1 mm area, suggesting locally high uniformity. For all the reported images in this manuscript, the interrogation wavelength was fixed and need not be tuned at each interrogation spot. Larger fields-of-view could be achieved by scanning the sample.

In Figure 4, *in vivo* images of a chorioallantoic membrane (CAM) of 5-day chicken embryo model are demonstrated. The capillary beds on the surface of the model can be easily imaged. The signal-to-noise ratio of *in vivo* images were measured ~35 dB. To the best of our knowledge, this is the first time that a FPI-based

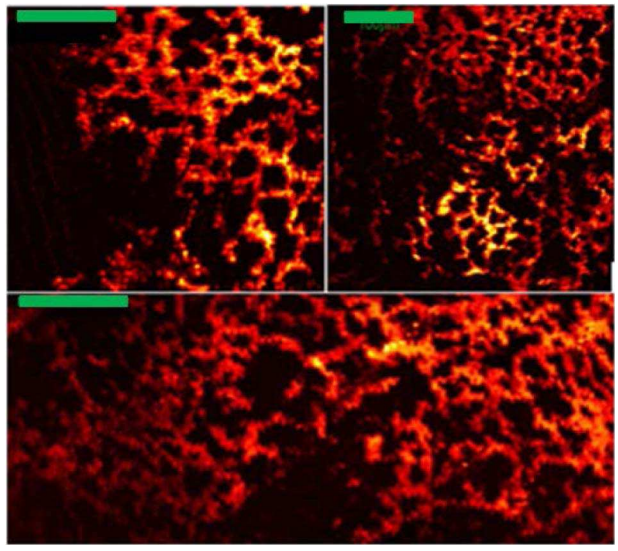

Fig. 4. *In vivo* images of capillary beds in the CAM-membrane of 5-day chicken embryo model. (Scale bar: 100 μm.)

reflection-mode optical-resolution PA technique is demonstrated for *in vivo* applications.

In summary a reflection mode OR-PAM using GLAD-FPI for *in vivo* imaging was demonstrated. The GLAD-based FPI was designed to form high-quality factor peaks in the C band range and transparent in the visible range wavelengths. The GLAD method allows low acoustic impedance FPI-device fabrication for highly sensitive ultrasound detection. High uniformity of the GLAD-FPI enables OR-PAM imaging using a fixed interrogation wavelength. A 532-nm excitation beam was combined by the integration beam and co-scanned and co-focused. Additional optimization of the focal positioning of interrogation beam into the etalon and excitation beam below the tissue surface could result in improved imaging.

We anticipate that the GLAD FPI could eventually pave the way for less expensive interrogation lasers with less stringent tuning requirements and for simultaneous recording of pressure signals at multiple different spatial locations with a single laser.

The first author gratefully acknowledges funding from the Killam Trust for an Izaak Walton Killam Memorial Scholarship, Alberta Innovates—Technology Futures, and Alberta Enterprise and Advanced Education for a Graduate Student Scholarship, University of Alberta for Dissertation fellowship, and Andrew Stewart Awards as well as SPIE for an SPIE Scholarship in Optics & Photonics. We also gratefully acknowledge funding from NSERC (355544-2008, 375340-2009, STPGP 396444), Terry Fox Foundation and the Canadian Cancer Society (TFF 019237, TFF 019240, CCS 2011-700718), the Alberta Cancer Research Institute (ACB 23728), the Canada Foundation for Innovation, Leaders Opportunity Fund (18472), Alberta Advanced Education & Technology, Small Equipment Grants Program (URSI09007SEG), Microsystems Technology Research Initiative (MSTRI RES0003166), University of Alberta Startup Funds, and Alberta Ingenuity/Alberta Innovates scholarships for graduate and undergraduate students. Also, MB and JS acknowledge funding from Alberta Innovates, NSERC, and Micralyne.

References

1. L. V. Wang, Scholarpedia **9**, 10278 (2014).
2. L. V. Wang and S. Hu, Science **335**, 1458 (2012).
3. E. Zhang, J. Laufer, and P. Beard, Appl. Opt. **47**, 561 (2008).
4. Z. Xie, S. L. Chen, T. Ling, L. J. Guo, P. L. Carson, and X. Wang, Opt. Express **19**, 9027 (2011).
5. S. Ashkenazi, Y. Hou, T. Buma, and M. O'Donnell, Appl. Phys. Lett. **86**, 134102 (2005).
6. S. Huang, S. Ashkenazi, Y. Hou, R. S. Witte, and M. O'Donnell, Proc. SPIE **6437**, 643728 (2007).
7. P. Hajireza, K. Krause, M. Brett, and R. Zemp, Opt. Express **21**, 6391 (2013).
8. H. Li, B. Dong, Z. Zhang, H. F. Zhang, and C. Sun, Sci. Rep. **4**, 4496 (2014).
9. S. Chen, Z. Xie, T. Ling, L. J. Guo, X. Wei, and X. Wang, Opt. Lett. **37**, 4263 (2012).
10. P. V. Chitnis, H. Lloyd, and R. H. Silverman, *Proceedings of IEEE Conference on International Ultrasonic Symposium* (IEEE, 2014), pp. 353–356.
11. M. M. Hawkeye, M. T. Taschuk, and M. J. Brett, *Introduction: Glancing Angle Deposition Technology, in Glancing Angle Deposition of Thin Films: Engineering the Nanoscale* (Wiley, 2014).
12. P. Hajireza, A. Forbrich, and R. J. Zemp, Opt. Lett. **38**, 2711 (2013).
13. W. Shi, S. Kerr, I. Utkin, J. Ranasinghesagara, L. Pan, Y. Godwal, R. J. Zemp, and R. Fedosejevs, J. Biomed. Opt. **15**, 056017 (2010).
14. P. Hajireza, W. Shi, and R. J. Zemp, Opt. Lett. **36**, 4107 (2011).
15. P. Hajireza, W. Shi, and R. J. Zemp, Opt. Express **19**, 20097 (2011).